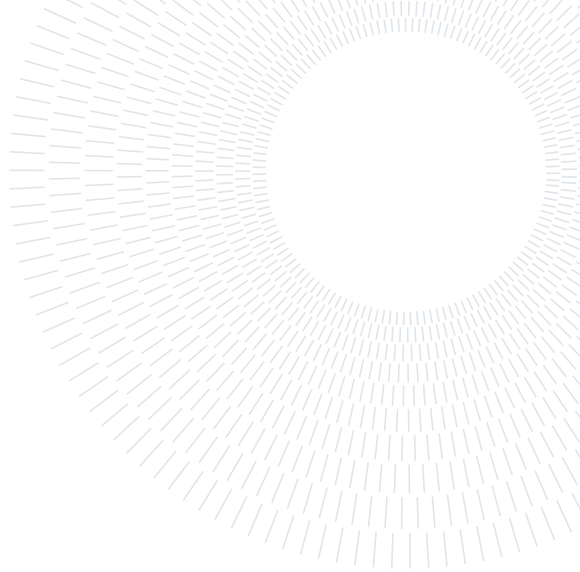




**POLITECNICO**  
MILANO 1863

SCUOLA DI INGEGNERIA INDUSTRIALE  
E DELL'INFORMAZIONE



## Course Report: Control of a Separately-Excited DC Motor for Tramway Applications

LAUREA MAGISTRALE IN AUTOMATION AND CONTROL ENGINEERING - INGEGNERIA DELL'AUTOMAZIONE

**Author:** MASSIMILIANO MIGLIORINI

**Advisor:** PROF. MARCO MAURI

**Co-advisor:** NICOLA TOSCANI

**Academic year:** 2024-2025

---

### 1. Introduction

#### 1.1. Problem Description

Tramway vehicles “Carelli 1928” by the ATM company (still in operation in Milan and San Francisco) are driven by four DC motors with series excitation.



In this report, we present a method to control the electric machine that moves the tram, assuming for simplicity that the four DC motors of the actual tram behave as a single, equivalent separately excited DC motor. Our objective is to design and simulate a speed controller for a 10 km route, characterized as follows:

distance [km]	slope %	speed
0 – 1	0	$v_r/2$
1 – 3	0	$v_r$
3 – 4	5	$v_r$
4 – 6	0	$v_{\max}$
6 – 8	0	$v_r$
8 – 9	-5	$v_r$
9 – 10	0	$v_r/2$

The excitation circuit parameters are:

- excitation rated voltage:  $V_{er} = 60$  V
- excitation rated current:  $I_{er} = 5$  A
- excitation resistance:  $R_e = 12 \Omega$
- excitation time constant:  $\tau_e = 0.1$  s

The equivalent-circuit parameters of the DC motor are:

- line voltage:  $V_{DC} = 600$  V
- rated power of each motor:  $P_r = 21$  kW
- maximum speed of the vehicle:  $v_{\max} = 42$  km/h
- rated speed of the motor:  $\Omega_r = \Omega_b = 970$  rpm
- overall rated current:  $I_{tot,r} = 156$  A
- torque constant:  $K_T = 1.06$  Nm/A
- armature resistance:  $R_a = 0.39 \Omega$
- armature circuit time constant:  $\tau_a = 10$  ms

Finally, the parameters used to model the tram's mechanical structure are:

- mass of the vehicle at no load:  $m_T = 15$  t
- maximum loading capacity: 130 passengers (80 kg each)
- diameter of the wheel:  $d = 680$  mm
- gearbox ratio (motor-to-wheels):  $\rho = 13/74$
- friction coefficient:  $\beta = 0.81$  Nms

## 1.2. Missing Parameters calculation

In the section below, we report all the equations used to retrieve the missing parameters relevant to our problem, based on the data listed in the previous section. These parameters will be used in the following parts of the report to build the model of the electric machine and to correctly implement the control scheme.

$L_e = \tau_e R_e$	Excitation inductance
$m_{\max} = m_T + 130 \cdot 80$	Total mass of the vehicle with 130 passengers (80 kg each)
$P_{r,tot} = 21000 \cdot 4$	Total rated power (4 motors, 21 kW each)
$\omega_{\max} = \frac{v_{\max}}{3.6} \cdot \frac{2}{d\rho}$	Maximum angular speed (mechanical limit)
$\omega_b = 970 \cdot \frac{2\pi}{60}$	Rated angular speed of the motor
$v_r = \omega_b \cdot \rho \cdot \frac{d}{2} \cdot 3.6$	Rated linear speed of the vehicle
$L_a = \tau_a R_a$	Armature inductance
$J = m_{\max} \cdot \left( \frac{\rho^2 d^2}{4} \right)$	Equivalent inertia seen from the motor shaft
$T_n = \frac{P_{r,tot}}{\omega_b}$	Nominal torque
$E_n = K_T \cdot I_{e,r} \cdot \omega_b$	Nominal back EMF

## 2. Control Scheme Description

In the following paragraphs we will see how to control a Separately Excited DC Motor, starting from the basic equations that describes the armature and excitation circuits, the mechanical part of the tram and also the additional contribute given by the resistant torque, which has to be taken into account when designing the control part.

The aim of this control scheme is to track the provided speed profile of the tram (reported in the previous section), ensuring that the speed targets are reached in a reasonable and "safe" manner, while avoiding rapid or oscillatory dynamics that could lead to mechanical vibrations or, even worse, instability.

The resulting control must also be robust to environmental noise; in our simplified case, the only external disturbance is a resisting torque that occurs in the sloped sections of the track.

### 2.1. Full Scheme

Below, we present the complete control scheme architecture to be implemented in Simulink for the DC motor control. In *Section 2.4*, each part of this scheme is explained in detail.

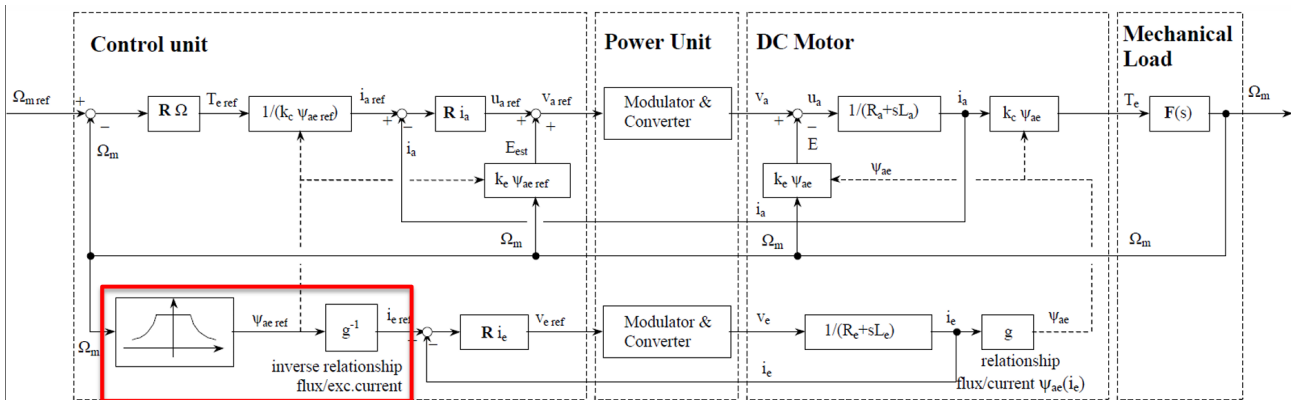


Figure 1: Complete block scheme for the DC motor control

## 2.2. DC Motor Equations and Excitation Circuit

### 2.2.1 System Equations

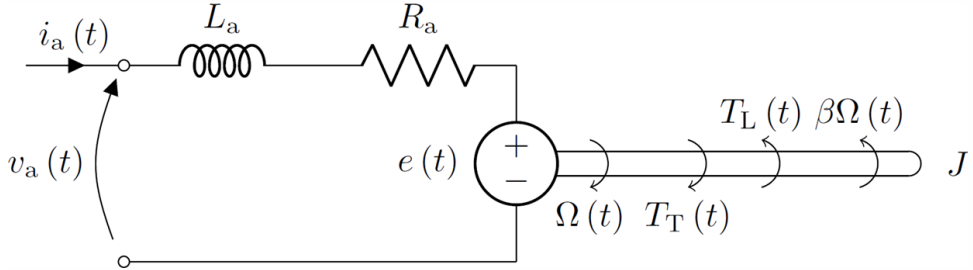


Figure 2: Circuit model with shaft connection

The DC motor (excluding the excitation circuit, which is discussed in *Section 2.2.3*) is described by two main differential equations:

Electrical equation (armature circuit):

$$v_a(t) = L_a \frac{di_a(t)}{dt} + R_a i_a(t) + e(t) \quad (1)$$

Mechanical equation (all quantities at the **motor side**):

$$T_T(t) - T_L(t) = J \frac{d\Omega(t)}{dt} + \beta \Omega(t) \quad (2)$$

Both equations represent first-order dynamics, which suggests using a simple PI controller architecture to regulate the machine, as presented in the following sections.

Note that the torque  $T_T(t)$  can be positive or negative because the tramway's DC motor provides an **electrical braking torque** without any additional mechanical brake in the control scheme.

Consequently, all mechanical and electrical variables involved in the control (such as  $T_T$ ,  $v_a$ , and  $i_a$ ) may assume **negative values**, extending their magnitude symmetrically about zero.

### 2.2.2 Mechanical Load

The resistant torque in this simplified model accounts only for the track slope. From the slope percentage in the data table for each segment, we compute the road inclination angle as:

$$\theta(t) = \arctan(\text{slope \%}).$$

The resistant torque is then:

$$T_{\text{res}} = M \cdot \left(\frac{d}{2}\right) \cdot g \cdot \sin(\theta(t)) \cdot \rho,$$

where  $M$  is the vehicle mass,  $d$  the wheel diameter,  $g$  gravitational acceleration, and  $\rho$  the gear ratio.

*NB: in this report we analyze the worst-case scenario statically by setting  $M = m_{\max}$ .*

### 2.2.3 Separate-Excitation Circuit

The separately excited field circuit is modeled as a simple series RL load, analogous to the armature circuit introduced above. Its dynamic behavior is governed by the following differential equation:

$$v_e(t) = L_e \frac{di_e(t)}{dt} + R_e i_e(t). \quad (3)$$

This circuit generates the stator excitation field  $B_{\text{exc}}$ , which is essential for the electromagnetic energy conversion within the DC motor.

In *Section 2.4.2* we'll see how to implement the Proportional-Integral current control for this simple first order system.

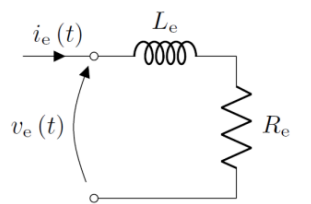


Figure 3: The Excitation Circuit

### 2.2.4 Mechanical Characteristic and Operating Regions

The extended mechanical characteristic of a separately excited DC motor is shown in *Figure 4*. This graph not only represents the torque  $T_e$  as a function of the motor's mechanical speed  $\Omega_m$ , but also relates the other key motor quantities to speed.

First, we distinguish between the concepts of **base speed** and **mechanically constrained maximum speed** of the rotor.

- **Base speed  $\Omega_b$ :** also known as the rated speed, this is the speed at which the armature voltage  $V_{an}$  reaches its maximum rated value.  $\Omega_b$  is not a mechanical limit; in fact, it can be exceeded by reducing the excitation flux, as discussed in *Section 2.4.2*.
- **Maximum mechanical speed  $\Omega_{m \max}$ :** this is a hard mechanical limit that cannot be surpassed—even with further flux reduction—to ensure the integrity of the machine's rotating components.

Having established this distinction, we can identify two principal operating regions, which have a significant impact on the design of the control scheme:

- **Constant-Torque Region:** all operating points below base speed fall within this region. Here, the torque is maintained at its rated value  $T_{e,\max}$  (or reduced if the operation so requires). Both armature and excitation currents (or flux) remain at their nominal values, while the armature voltage and back EMF increase linearly with speed—according to the motor equations—to sustain constant torque.
- **Constant-Power Region:** beyond base speed, the excitation flux  $\psi_{ae}$  is progressively reduced in proportion to the inverse of speed, allowing higher speeds to be reached. Although armature current and voltage stay at nominal levels, the available torque decreases, which limits acceleration and responsiveness (as will be further discussed in the central section on traction, e.g., the tram route).

The use of both regions is typical in traction applications (such as tram vehicles), where high starting torque is required, followed by efficient high-speed operation with reduced torque in the field-weakening region.

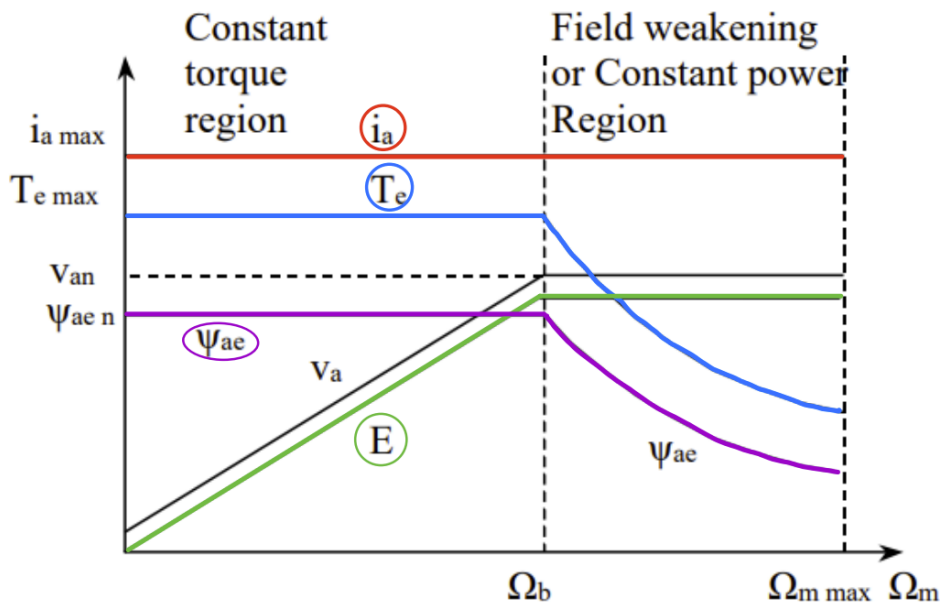


Figure 4: Operating Regions (*considering only the positive part, for clarity*)

### 2.3. Power Converter Unit

In our simplified study case analysis we can assume that the power converter ("Modulator & Converter", in the block scheme) has no dynamic, thinking about it as "so fast" that instantly gave us the desired conversion. Due to this fact, we can basically neglect it in the control design phase.

In case we want to represent its dynamic, we can just include a pure delay as its transfer function.

## 2.4. Control Unit (theoretical principles of control)

In the following sections we'll see the principles of the **cascade control** applied to the DC motor machine, highlighting its applicability conditions and the advantages of this principle in the design phase. At the end we'll focus on the usual working conditions for the excitation circuit and the assumptions used.

### 2.4.1 Speed and Armature Current Control

The DC motor inherently exhibits a coupled dynamic (visible in the red-highlighted section of *Figure 5*) since the back EMF  $E$  enters the current feedback loop and mixes mechanical and electrical quantities, rendering a fully decoupled cascade control impractical. To enable independent design of the two PI controllers, we include an *estimate of the back EMF*, computed from the reference excitation current and rotor speed:

$$E_{\text{est}}(t) = K_S i_{e,\text{ref}}(t) \Omega_m(t).$$

After introducing this estimate, the PI gains  $\{K_p, K_i\}$  can be tuned independently by examining the corresponding transfer functions.

This back EMF estimation also prevents the generation of a high (and potentially dangerous) braking current in case of a **fault in the digital control system**. If the PI controllers are reset for any reason, they would otherwise drive the armature voltage  $V_a$  to zero (causing high losses). Using  $E_{\text{est}}$  as the voltage reference allows a safer controller re-engagement.

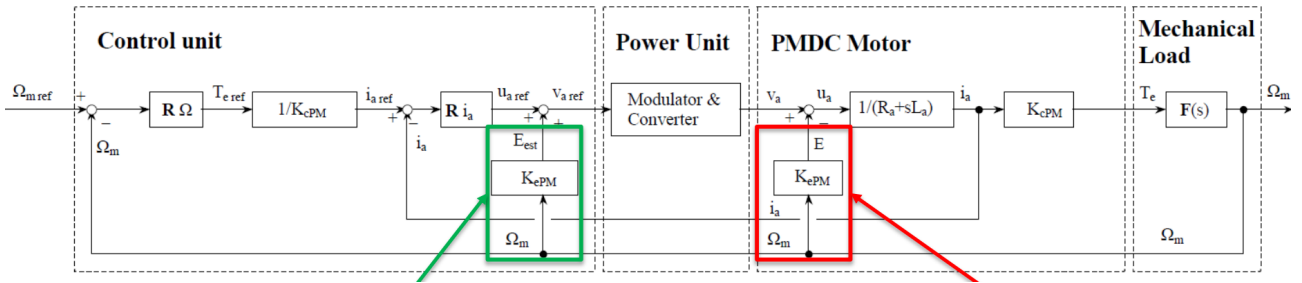


Figure 5: Actual EMF in the model equations (red) and its estimate (green)

We implement the motor control using cascaded PI loops, each tuned to its respective first-order subsystem. The general PI controller is given by

$$\text{PI}(s) = K_p + \frac{K_i}{s}.$$

The design methodology for selecting  $K_p$  and  $K_i$  is detailed in *Section 3.0.1*.

Finally, this cascaded decoupled control approach is valid only if the mechanical time constant  $\tau_{\text{mec}}$  is significantly larger (at least ten times) than the electrical time constant  $\tau_{\text{ele}}$ . Therefore, during controller design (*Section 3.0.1*), we impose  $\tau_{\text{mec}} \approx 10 \tau_{\text{ele}}$  ensuring that the outer mechanical loop sees the current loop as nearly instantaneous.

### 2.4.2 Excitation Circuit Control

The structure of the separately excited control allows us to independently regulate the excitation current, given a reference angular speed. In this section, we present the fundamental relationships that enable the generation of the excitation field  $B_{\text{exc}}$  through the flux/current relationship.

First, we consider only the linear region of the magnetizing curve, where the relationship between excitation current  $i_e$  and excitation flux is

$$\psi_e = K_s i_e. \quad (4)$$

Although this expression is often written using  $L_e$  instead of  $K_s$ , if the ferromagnetic material is linear and exhibits no hysteresis, the inductance coincides with the proportionality constant  $K_s$ , which is experimentally determined and provided in the data under the name  $K_T$ .

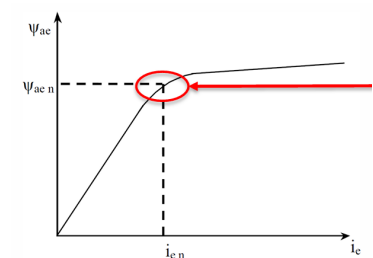


Figure 6: Nominal operating point: "knee" of the magnetizing curve

We can then define the two main relationships that connect the excitation system to the other quantities of the DC motor:

$$e(t) = K_S i_e(t) \Omega(t), \quad (5)$$

$$T_T(t) = K_S i_e(t) i_a(t). \quad (6)$$

In conclusion, to optimize the energy conversion process, we select the "knee" of the magnetizing curve (shown in *Figure 6*) as the operating point, where the linear approximation remains valid.

As illustrated in *Figure 7*, the excitation control strategy is divided into two regions:

- **Below base speed:** the excitation current reference  $i_{e,\text{ref}}$  is set to its rated value  $i_{e,\text{max}}$ , maintaining constant excitation flux.
- **Above base speed:** the excitation flux must be reduced in proportion to the inverse of the rotor speed,  $\psi_e \propto 1/\omega$ , which consequently reduces the maximum torque available.

The output of this excitation block enters the machine model as described by the equations above and is essential for estimating the back EMF.

In *Section 4.3*, we present the implementation of the excitation system control within the block diagram.

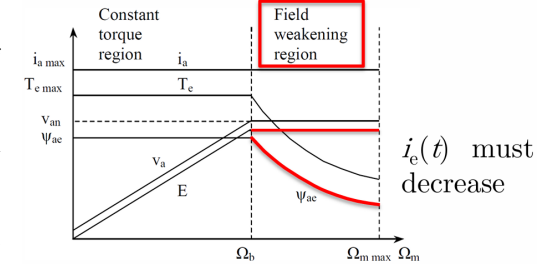


*Figure 7: Excitation flux regulation below and above  $\Omega_b$*

### 3. PI Controllers Implementation

#### 3.1. Tuning of $\{K_p, K_i\}$ Parameters

To set the PI gains, we use MATLAB's *pidtune* function. First, we express the three transfer functions of the system by translating the equations from *Sections 2.2.1* and *2.2.3* into the Laplace domain. Each of them represent a first-order system analogous to an RL load.

Next, we specify the desired crossover frequencies  $\omega_c$  for the three loops. To achieve a **decoupled** cascade control, the mechanical time constant must satisfy  $\tau_{\text{mec}} \approx 10 \tau_{\text{ele}}$ . By selecting  $\omega_c$  accordingly, the inner current loop appears “infinitely fast” to the outer speed loop, allowing independent design. We verify decoupling by comparing the Bode plots of the speed-only closed-loop transfer function  $F_{\text{speed}}(s)$  and the cascaded transfer function  $F_{\text{comp}}(s)$ . Similar low-frequency behavior confirms successful decoupling.

We chose:

- $\omega_{c,\text{mecc}} = 5 \text{ rad/s}$  (mechanical)
- $\omega_{c,\text{ele}} = 500 \text{ rad/s}$  (armature electrical)
- $\omega_{c,\text{exc}} = 50 \text{ rad/s}$  (excitation)

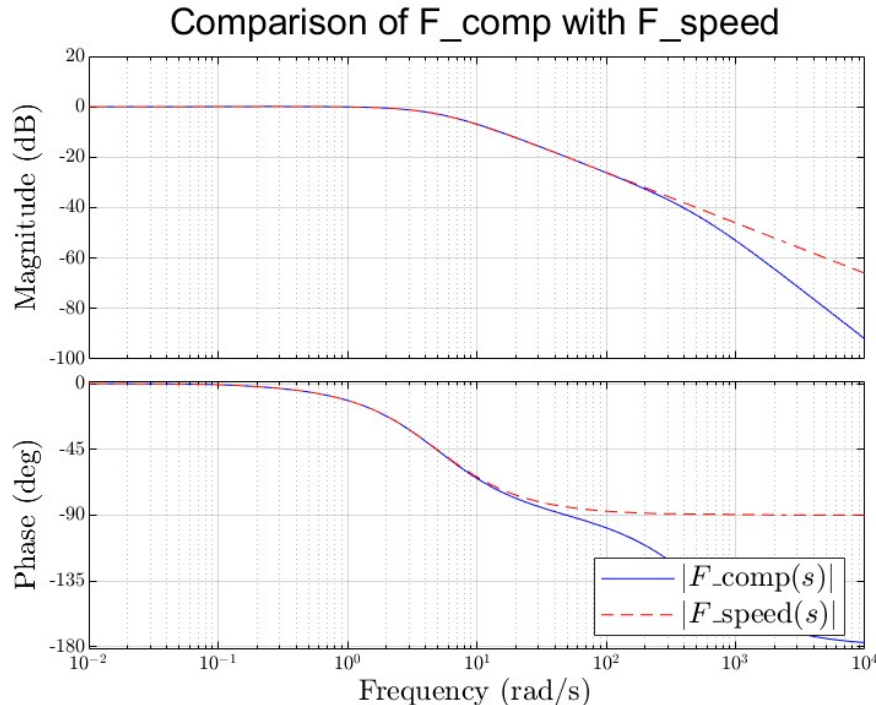


Figure 8: Bode comparison: speed loop alone vs. full cascaded loop

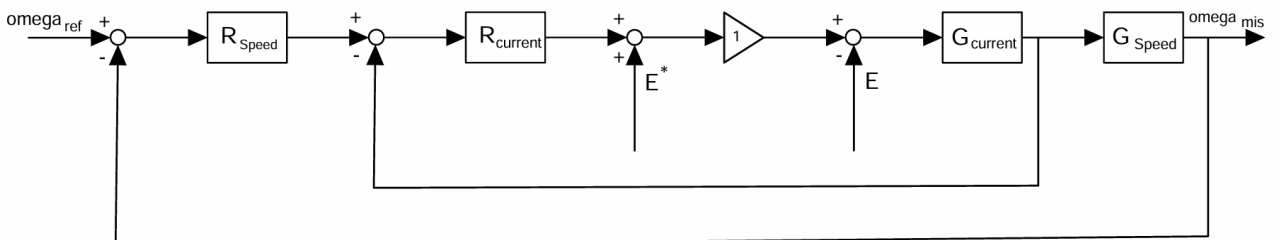


Figure 9: Equivalent decoupled scheme  $F_{\text{comp}}(s)$

Finally, we assign phase margins  $\varphi_m \geq 80^\circ$  to ensure stability and avoid oscillations. Here we idealize with  $\varphi_m = 90^\circ$  for all loops, noting that real-world specifications may require adjusted margins.

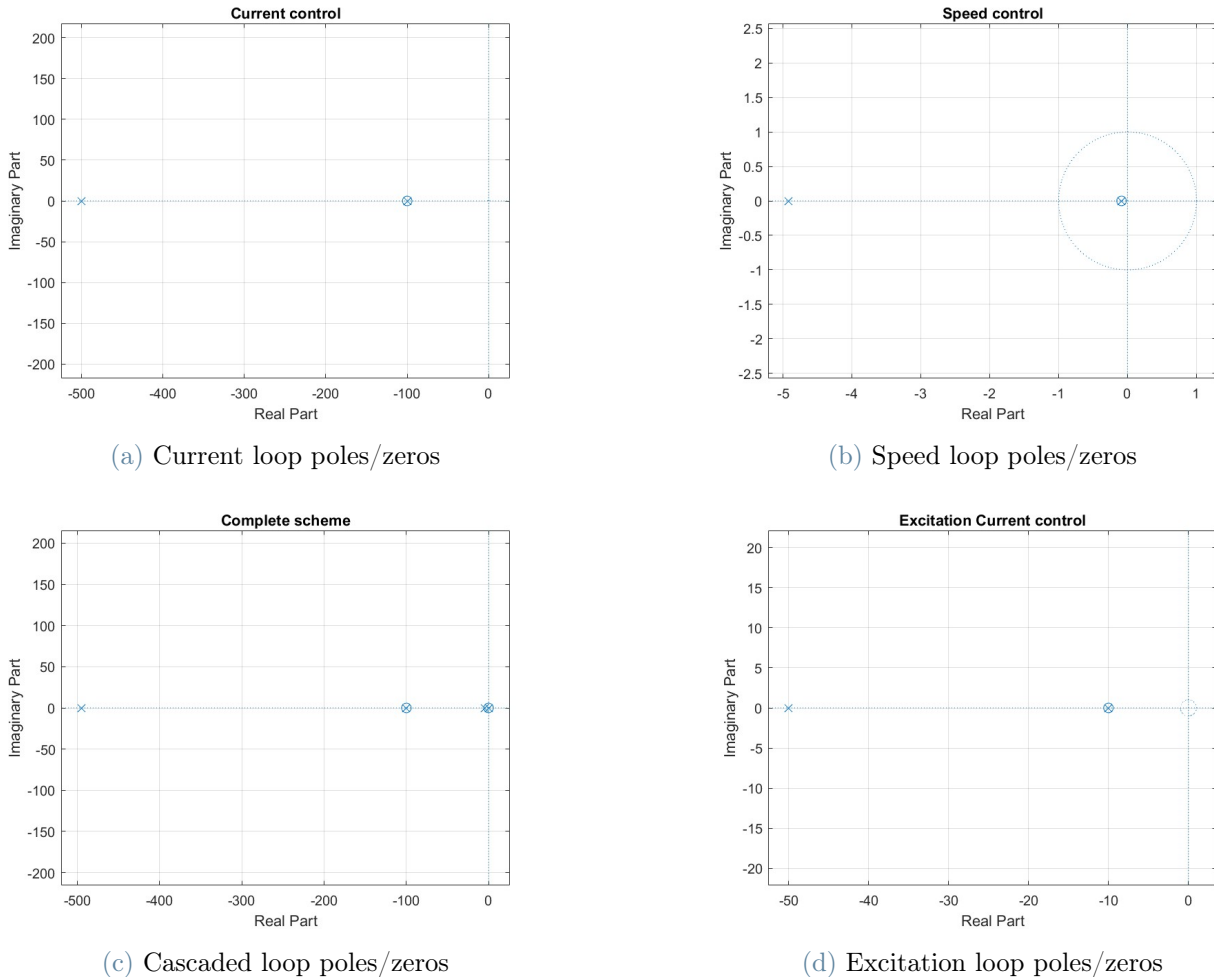
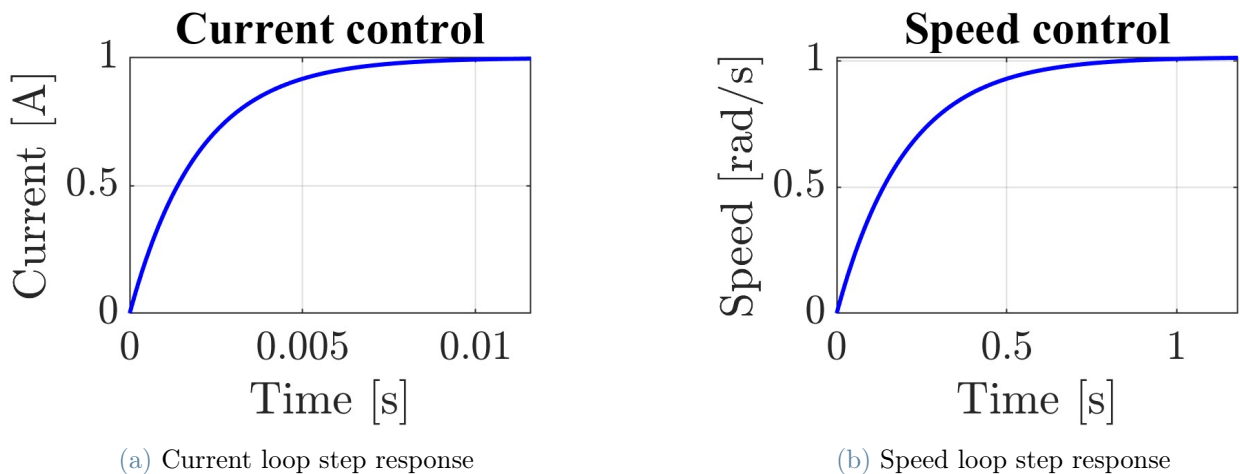
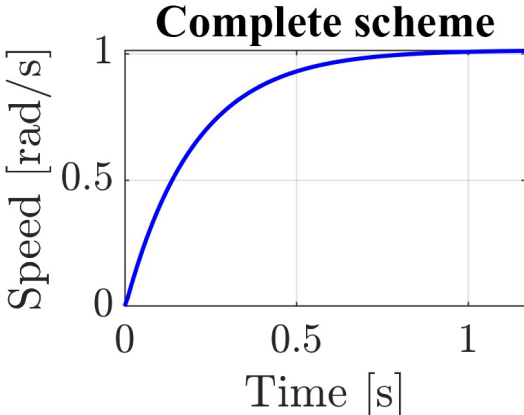


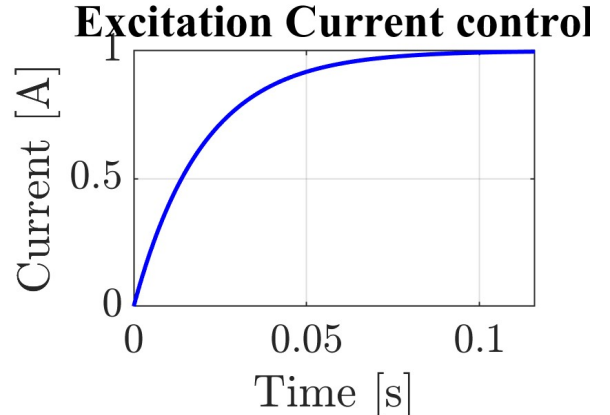
Figure 10: Pole-zero maps for the four control loops

With these settings, we call *pidtune* to compute  $\{K_p, K_i\}$ . We then validate by plotting step responses to confirm well-damped dynamics and negligible overshoot under the ideal  $\varphi_m = 90^\circ$ , as we can see in figures below.





(a) Cascaded loop step response



(b) Excitation loop step response

Figure 12: Step responses of the four control loops

The final result is an expression for each one of the three PI controllers of this type:

$$\text{PI}(s) = K_p + \frac{K_i}{s}.$$

### 3.2. Implementation of the Anti-Windup Scheme

In our control architecture, it is necessary to introduce the concept of *actuator saturation*, defined as the maximum physical output available for a given input demand. This limitation may arise from two sources: the actuator's rated performance (as specified by the manufacturer) or the physical constraints of the system. Both limits are typically listed in the machine's datasheet.

To prevent the PI controllers from requesting control actions beyond these limits, we incorporate an anti-windup mechanism by **saturating the integral action**. Without anti-windup, the integrator continues to accumulate error during saturation, causing excessive overshoot and prolonged recovery when the actuator returns to its linear region. The effect on system dynamics is shown in *Figure 14*.

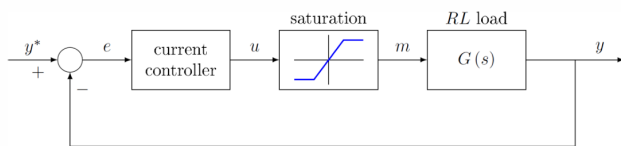


Figure 13: Actuator saturation in the control scheme

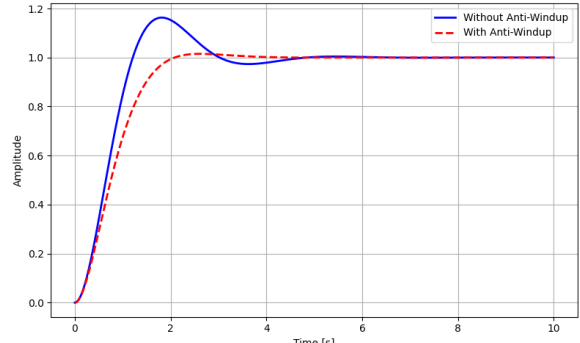


Figure 14: Improvements in the step response using the anti-windup configuration

In our application, the signals subject to saturation and their limits (as enforced in the PI controllers) are:

- **Torque reference**  $-T_n \leq T_{\text{ref}} \leq T_n$ , with the exception of the startup phase (which is assumed to occur only when the speed, starting from zero, is below 1.5 m/s), where we have  $-3T_n \leq T_{\text{ref}} \leq 3T_n$
- **Armature Voltage**  $-V_{\text{DC}} \leq V_a \leq V_{\text{DC}}$
- **Excitation Voltage**  $-V_{e,n} \leq V_e \leq V_{e,n}$

We implement a *back-calculation* anti-windup algorithm, which feeds the difference between the saturated actuator output and the controller's raw (unsaturated) output back into the integrator via a corrective gain (see *Figure 15*). A Simulink implementation of actuator saturation using switches is shown in *Figures 17 and 18*.

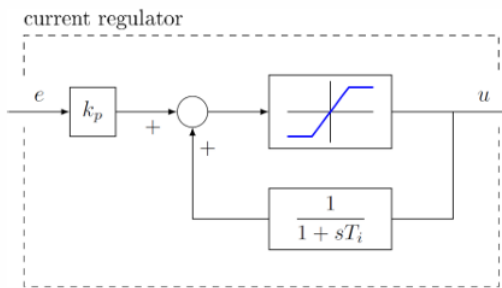


Figure 15: Control block with back-calculation anti-windup

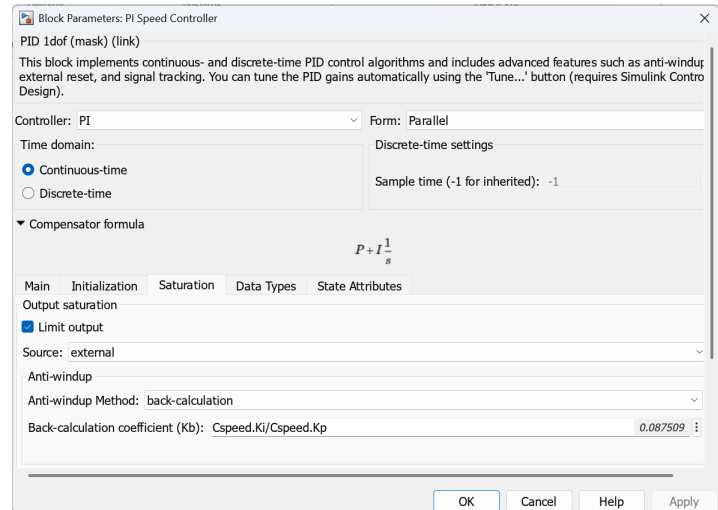


Figure 16: Simulink PI controller parameters for saturation

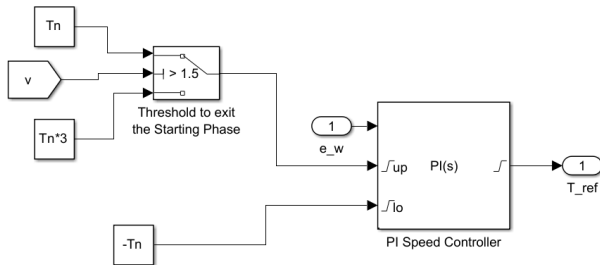


Figure 17: Mechanical torque saturation

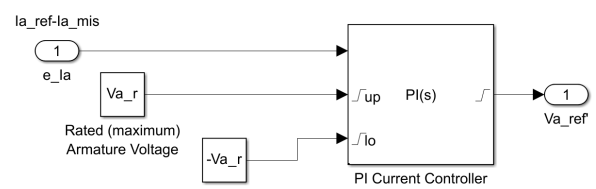
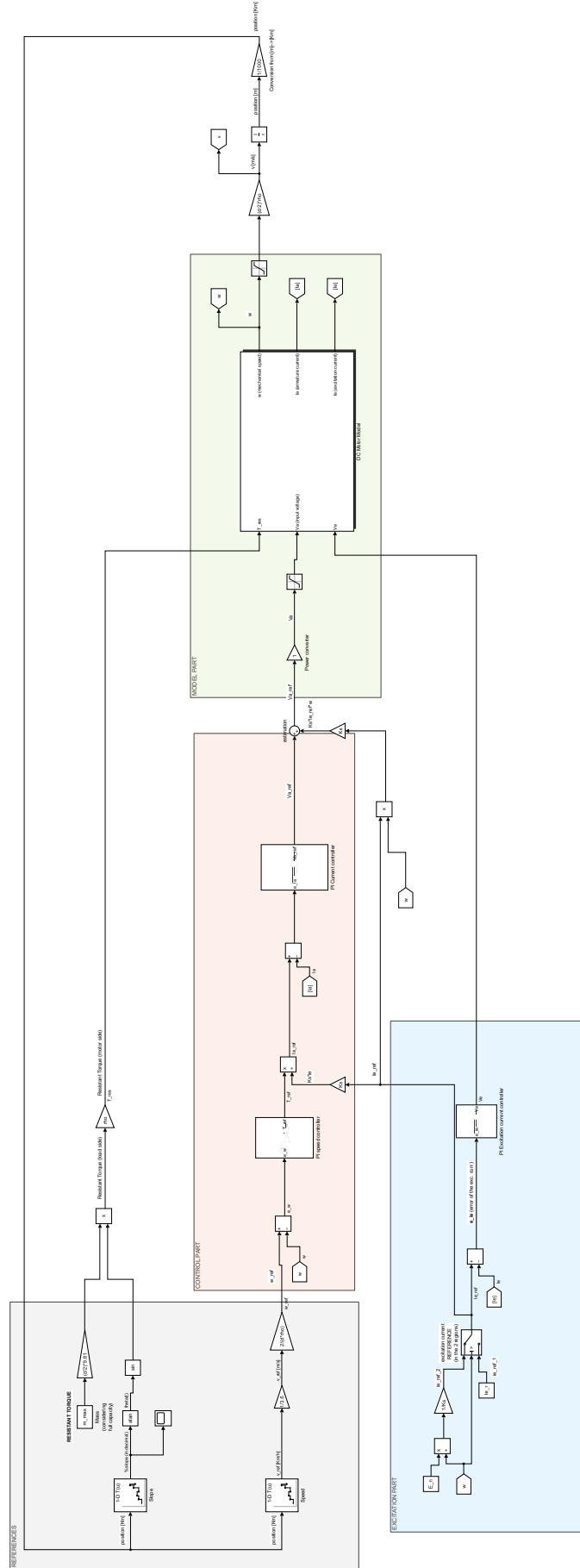


Figure 18: Armature voltage saturation

## 4. Simulink Model



## 4.1. References: Speed, Slope and Resistant Torque

### 4.1.1 Lookup Tables for Speed and Slope

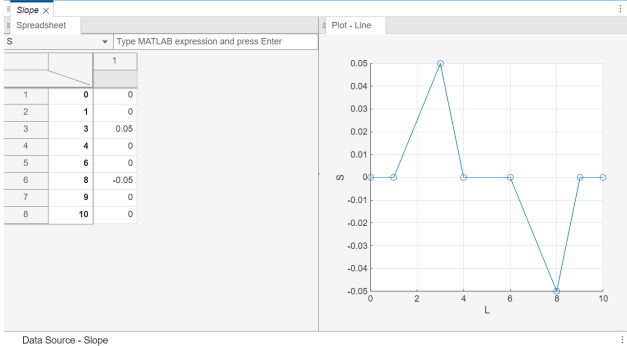


Figure 19: Slope lookup table

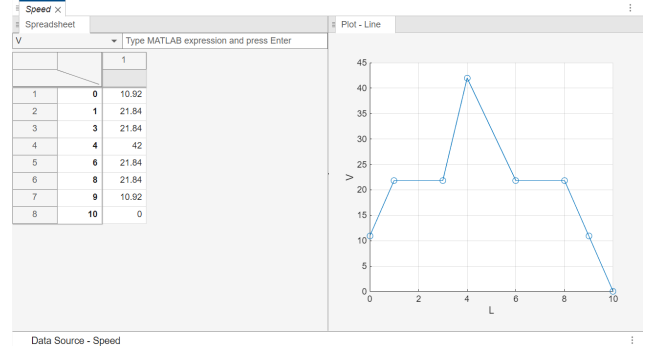


Figure 20: Speed lookup table

We can use the *Lookup Table* block to import the linear speed and slope percentage references into the Simulink control scheme, mapping input distance (in km) to outputs based on predefined data points. As shown in *Figures 19 and 20*, it suffices to replicate the dataset from *Section 1.1* in Simulink.

The linear speed reference  $v_{\text{ref}}$  is converted to rotor angular speed  $\omega_{\text{ref}}$  using:

$$\omega_{\text{ref}} = \frac{1}{3.6} \frac{2}{d\rho} v_{\text{ref}} \quad [\text{rad/s}],$$

where  $d$  is the wheel diameter and  $\rho$  is the gear ratio.

The slope percentage (expressed as a decimal) is converted to an inclination angle  $\theta(t)$  via

$$\theta(t) = \arctan(\text{slope \%}).$$

To determine the resistive torque  $T_{\text{res}}$ , we can include the vehicle mass  $m$  as an input reference. In our design, we consider the **worst-case scenario** with the tram fully loaded (mass  $m_{\text{max}}$ ). By applying the formula from *Section 2.2* with  $m = m_{\text{max}}$ , we obtain  $T_{\text{res}}$ . In a real-time implementation, the mass reference can be updated dynamically based on passenger load estimates.

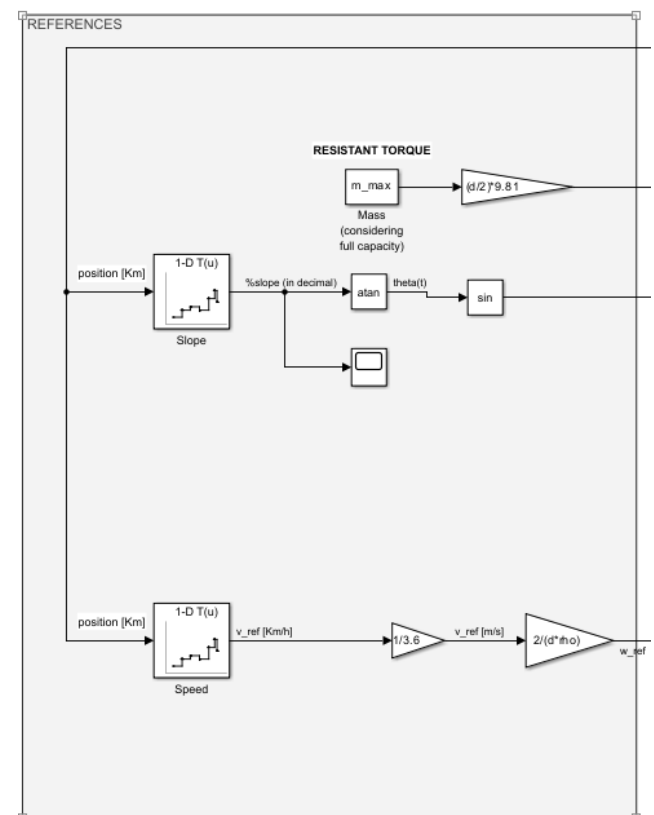


Figure 21: Reference signals in the block scheme

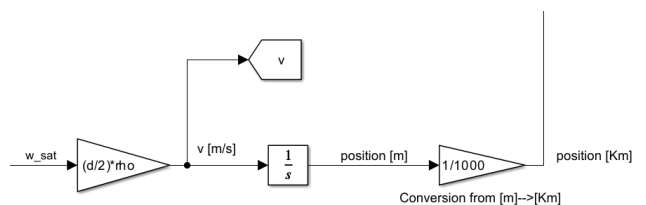


Figure 22: Conversion of position (km) to reference signals

#### 4.1.2 Resistant Torque at the Motor Side

In the image below is shown the plot of the resistant torque, which matches our expectations.

In our simplified case, the resistant torque is zero when the track is flat, neglecting other resistive effects (e.g. air resistance). The value of  $T_{\text{res}}$  is positive when the tram is going uphill and negative when it is going downhill.

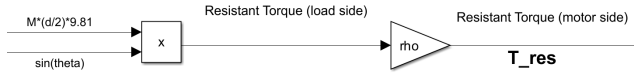


Figure 23: Block scheme translation of the  $T_{\text{res}}$  formula

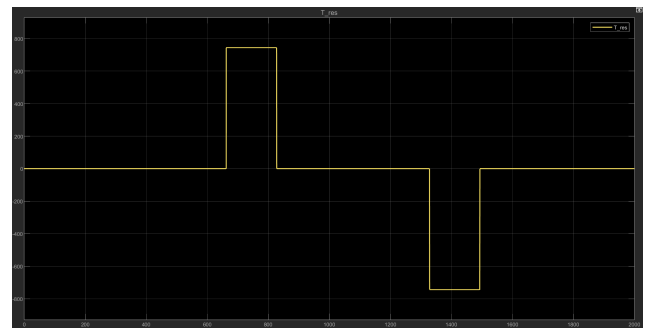


Figure 24: Evolution of  $T_{\text{res}}$  along the track

#### 4.2. Control Part (& plots of the controllers' output)

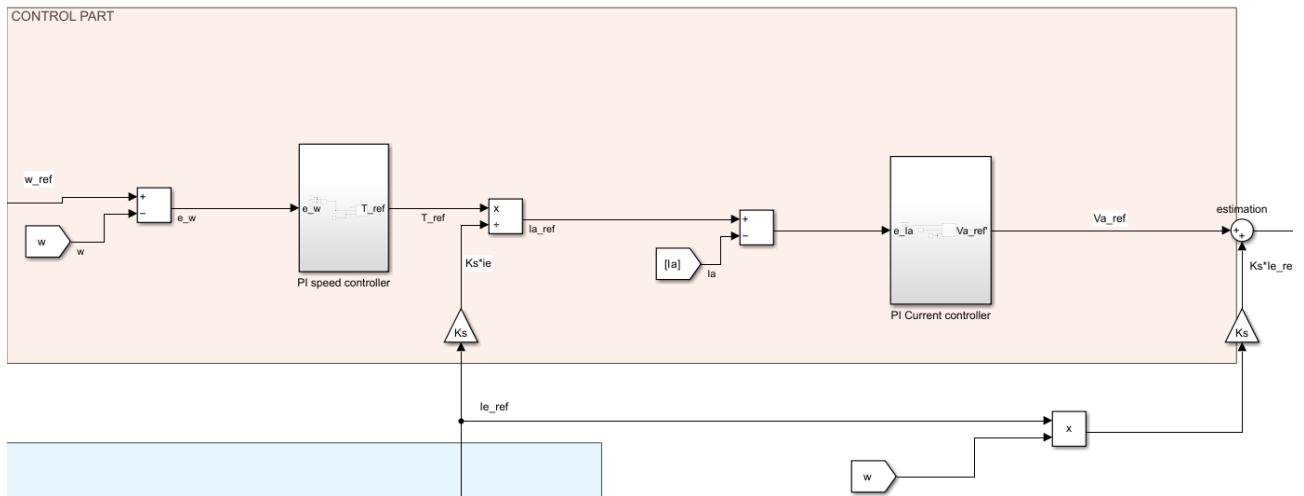


Figure 25: Control part in the block scheme

As discussed in previous sections, we operate using an **electrical braking torque**, internally provided by the DC motor. Consequently, we also observe negative values of the resistant torque, saturated as reported in *Section 3.0.2*.

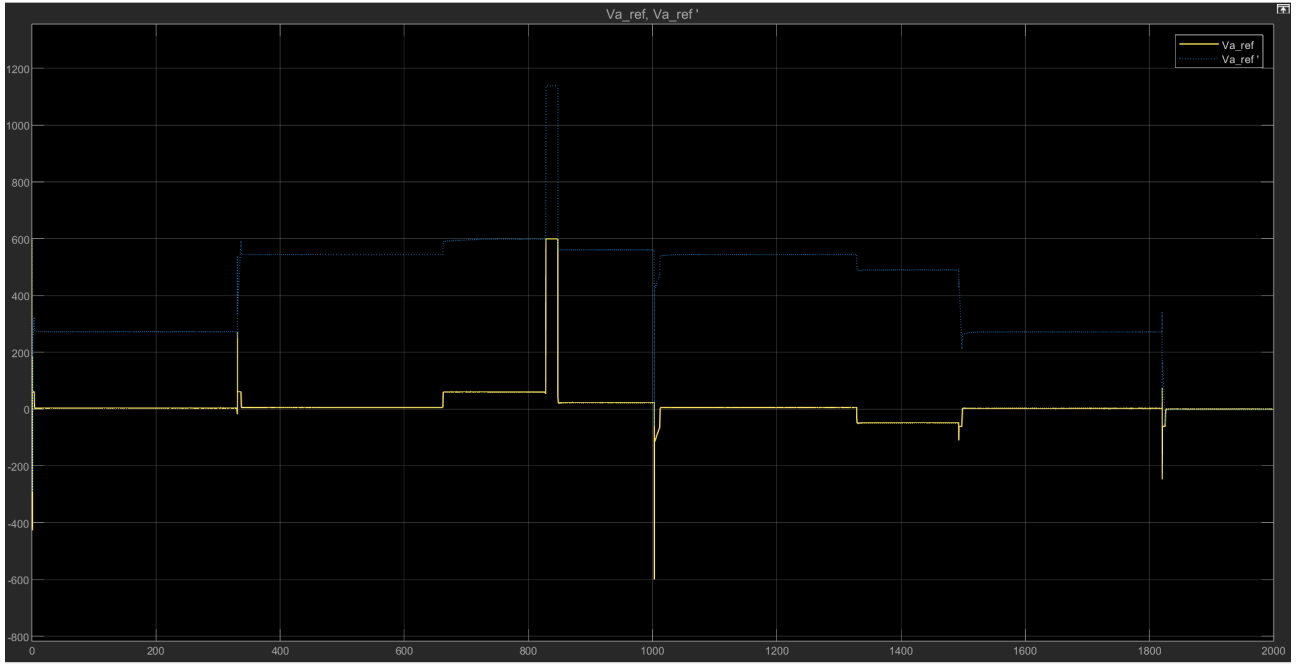


Figure 26: Saturated output of the armature current controller ( $V_{a,\text{ref}}$ , yellow line) and the “modified reference”, including the estimation ( $V'_{a,\text{ref}}$ , blue dashed line)

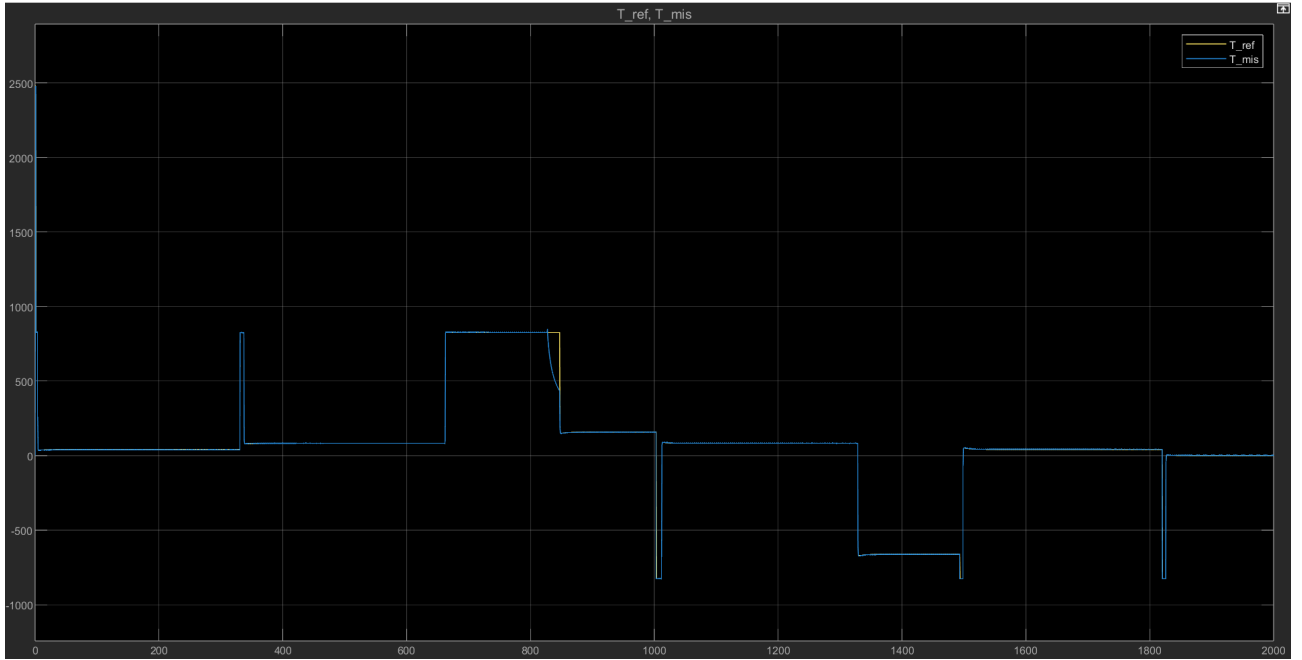


Figure 27: Mechanical torque: saturated reference output of the speed controller ( $T_{\text{ref}}$ , yellow line) and the actual torque applied to the system ( $T_{\text{mis}}$ , blue line)

In the center of the torque plot, we can observe a “hole” (see Figure 27), which corresponds to the transition into the constant-power region. As seen in the armature current and voltage plots, the armature voltage is saturated at its maximum value ( $V_{a,\text{max}} = 600 \text{ V}$ ). At  $t = 827.4 \text{ s}$ , the controller demands a speed above the base speed. Because both armature voltage and current remain fixed under saturation, the available torque decreases in accordance with the inverse relationship between torque and speed in the field-weakening region of the torque-speed characteristic. Thus, the behavior is as expected.



Figure 28: Torque behaviour when  $\omega > \omega_{\text{base}}$

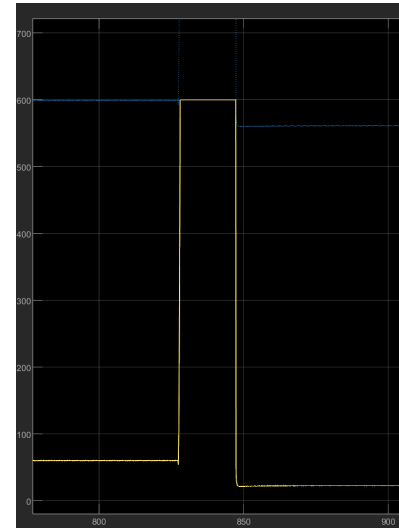


Figure 29: Armature voltage behaviour when  $\omega > \omega_{\text{base}}$

### 4.3. Excitation Part

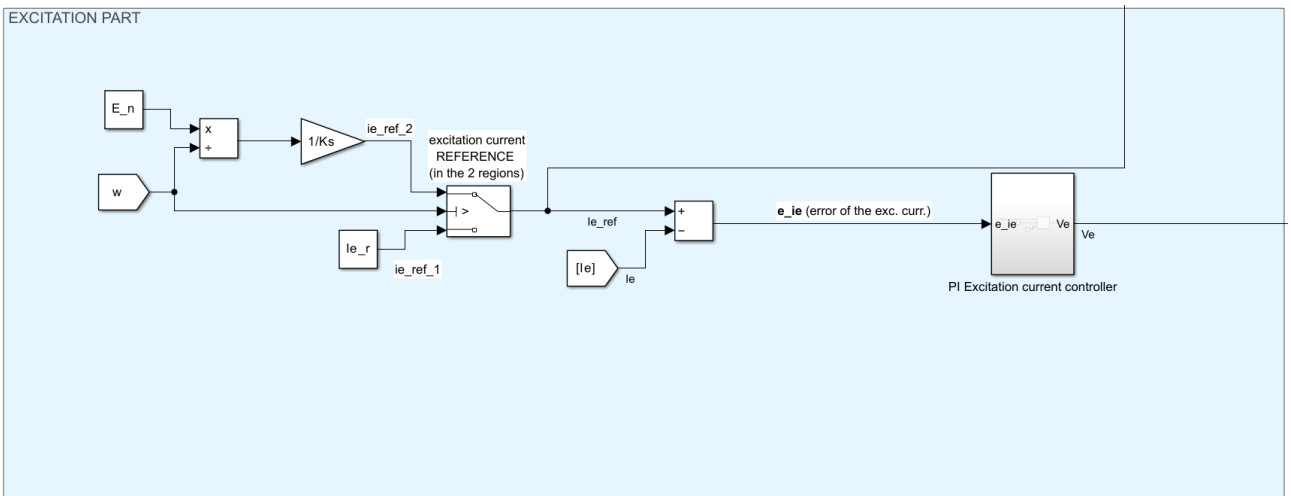


Figure 30: Excitation part in the block scheme

The excitation is controlled according to the behavior presented in the operating regions (*Section 2.2.4* and *Section 2.4.2*):

- **Below base speed:** we maintain the excitation voltage constant at its rated value  $V_{en}$ , using the rated excitation current  $i_{en}$  as reference.
- **Above base speed:** we reduce the excitation voltage proportionally to the inverse of mechanical speed, setting the reference to

$$i_{e,\text{ref}}(t) = \frac{E_n}{K_s \omega(t)}.$$

As expected, the only region where the excitation flux must be reduced is the central one, where the tram exceeds its base speed.

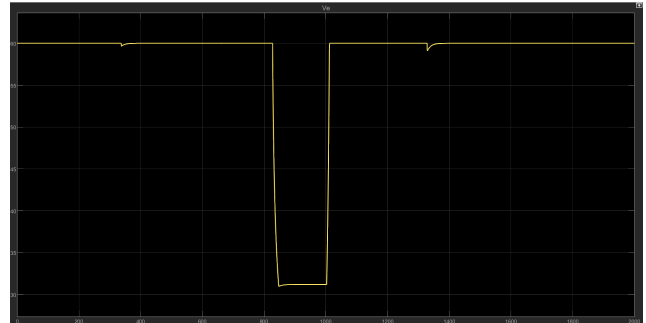


Figure 31: EXCITATION VOLTAGE: Saturated output of the Excitation Current controller ( $V_e$ )

#### 4.4. Model Part

According to the motor's equations, we have  $\{T_{\text{res}}, V_a, V_e\}$  as inputs and  $\{\omega, i_a, i_e\}$  as outputs of the model.

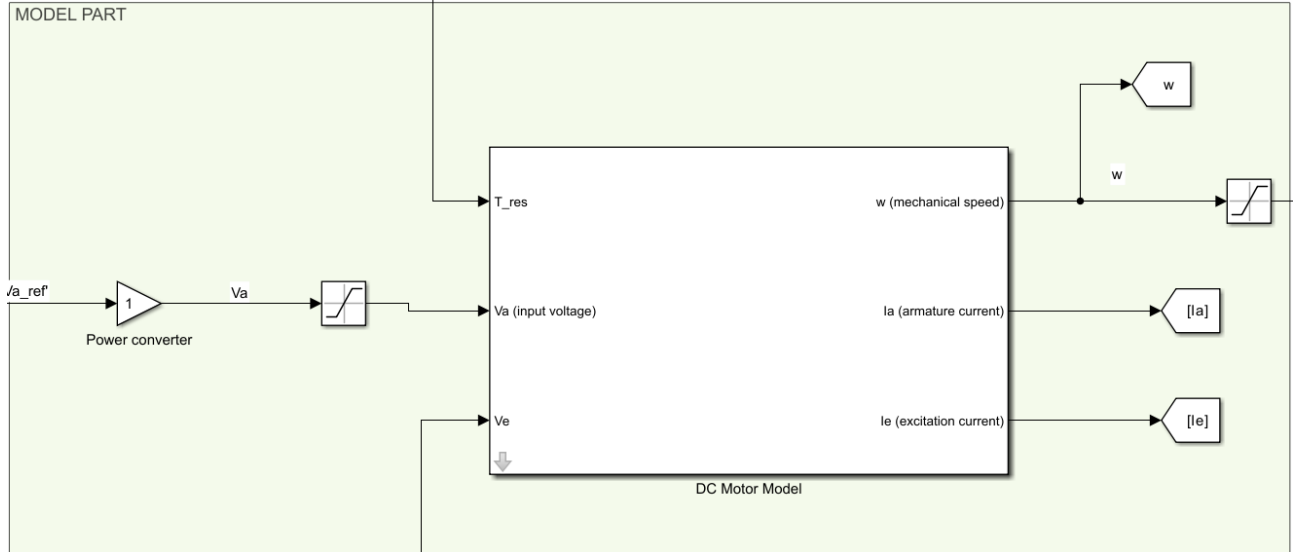


Figure 32: Inputs/Outputs of the DC motor

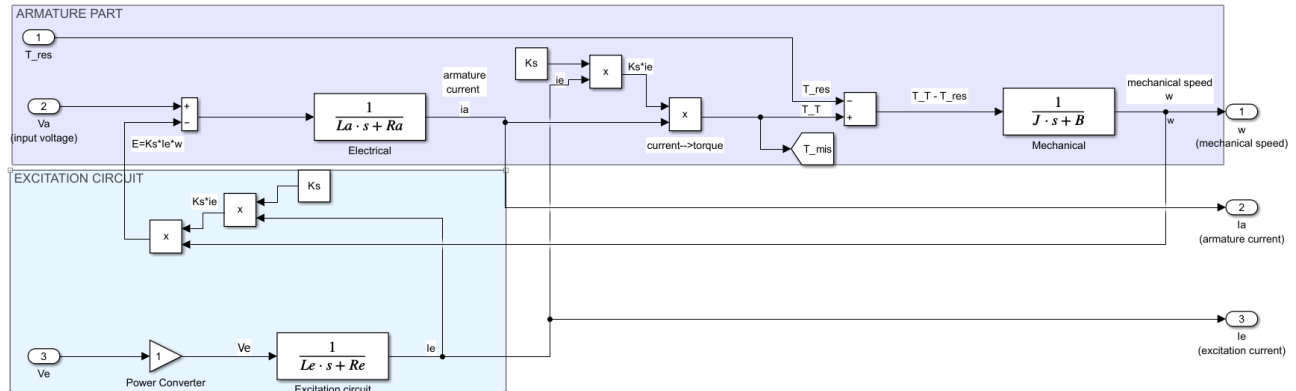


Figure 33: Block scheme representation of the *DC motor model*

We note that it is necessary to saturate the armature voltage  $V_a$  as it enters the DC motor model. Although the controller's output  $V_{a,\text{ref}}$  is already limited by a saturation block, the addition of the back-EMF estimation causes the total reference  $V'_{a,\text{ref}} = V_{a,\text{ref}} + E_{\text{est}}$  to potentially exceed the physical limit. For this reason, a second saturation block is added right after the estimation, ensuring that  $V_a$  is brought back within acceptable values before being applied to the motor.

This limitation imposed by  $V_{a,\text{max}}$  corresponds to a mechanical constraint that must be strictly respected at all times, since exceeding it may damage the motor's insulating gaskets (responsible for electrical isolation). As for the outputs, we highlight the need to implement at least three sensors in our system in order to provide the required measurements and enable the feedback control strategy to operate properly.

It is also important to saturate the angular speed  $\omega$  in output to a value  $\omega_{\text{sat}} > 0$ , as reverse motion is not allowed for the tramway vehicle and is not meaningful for our task. This means that the linear speed must always remain nonnegative. However, it is crucial *not* to use  $\omega_{\text{sat}}$  as the reference for control: in the last part of the trajectory, the controller might try to drive  $\omega$  to negative values. If we were to use this already-saturated value as reference, no corrective action would be applied and the system would fail to converge.

Below we report the resulting armature voltage, obtained with our control strategy:

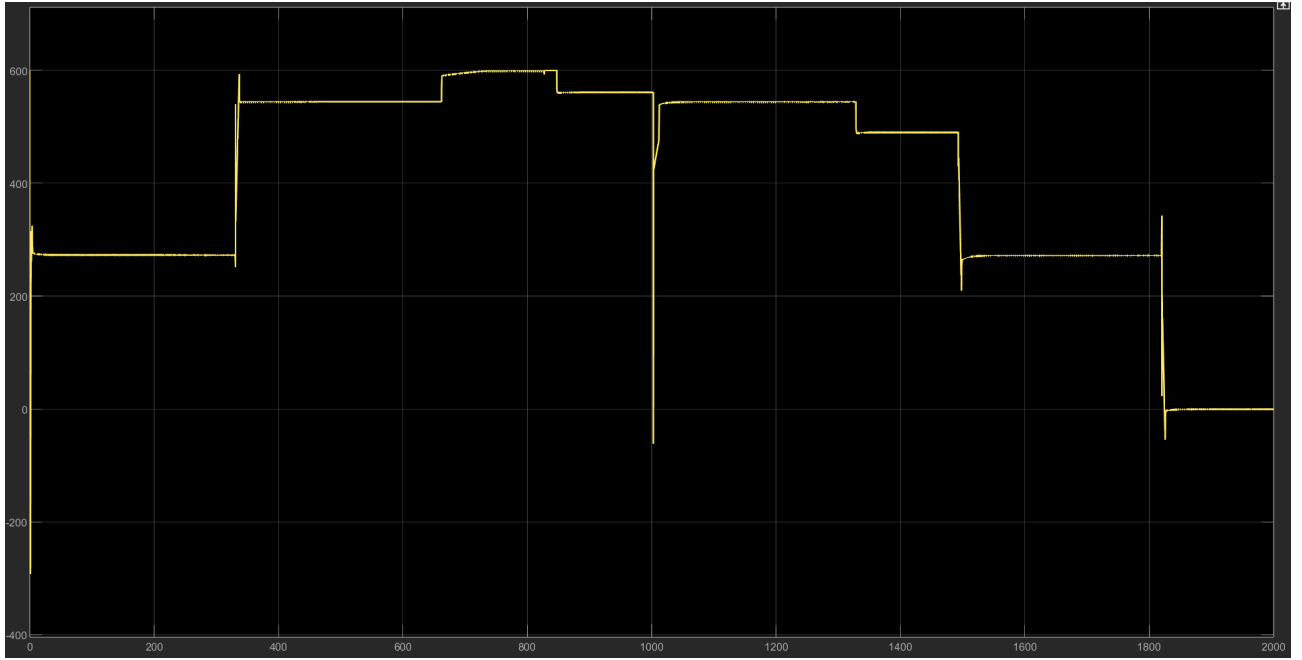


Figure 34: ARMATURE VOLTAGE: Actual saturated value of  $V_a$  that goes in as input of the DC motor

## 5. Results and Final Comments

### 5.1. Linear Speed Control

The following plot shows the primary task result: tracking the linear speed profile along the 10 km route. As shown, the controller tracks the reference accurately in the presence of slopes and during decelerations, thanks to the integrated electrical braking torque.

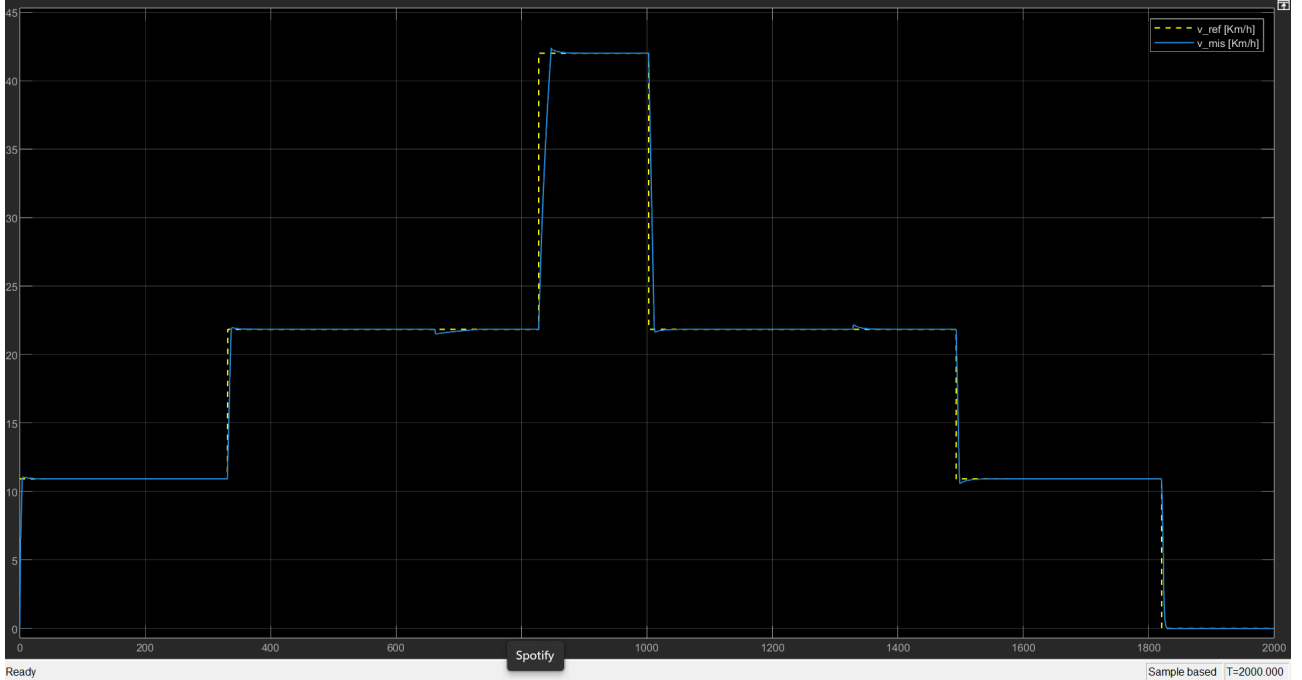


Figure 35: Desired linear speed profile to follow (dashed yellow line) Vs. measured linear speed (blue line), obtained with the control scheme

The **overshoot** in response to the speed step input is minimal, ensuring a fast reaction without oscillations while avoiding excessively aggressive control action. Additionally, to ensure that our control strategy is physically

feasible for a standard tramway vehicle, we examine the acceleration/deceleration values reached in different parts of the track.

Research online for the ATM “Carelli 1928” tramway vehicle indicates feasible acceleration values in the range  $[0.7 \text{ m/s}^2, 1.0 \text{ m/s}^2]$  during start-up, decreasing to approximately  $0.3 \text{ m/s}^2$  as the vehicle approaches its maximum speed.

Considering the “worst-case scenario” with  $0.7 \text{ m/s}^2$  at start and  $0.3 \text{ m/s}^2$  near maximum speed, we compute expected acceleration times for two speed ranges:

- $t_{\text{acc\_exp\_1}} = 4.4 \text{ s}$  for  $0\text{--}11 \text{ km/h}$
- $t_{\text{acc\_exp\_2}} = 18.6 \text{ s}$  for  $22\text{--}42 \text{ km/h}$

We can verify that the results from our control scheme align with these expectations. As shown in the plots below, the measured values closely match the expected ones.

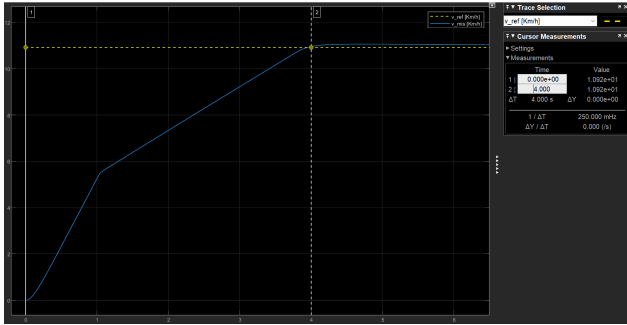


Figure 36: Measured acceleration time  
 $t_{\text{acc\_mis\_1}} = 4.0 \text{ s}$  for  $0\text{--}11 \text{ km/h}$

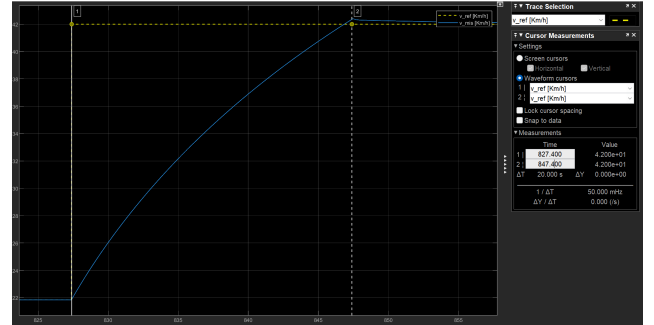


Figure 37: Measured acceleration time  
 $t_{\text{acc\_mis\_2}} = 20.0 \text{ s}$  for  $22\text{--}42 \text{ km/h}$

## 5.2. Armature Current Control

The armature current is regulated according to the torque required to achieve the desired motion of the tram. Recalling the relationship between armature current and torque:

$$T_{\text{mecc}} = K_S \cdot i_e(t) \cdot i_a(t) \quad (7)$$

As expected, current "peaks" occur when the tram must reach a new speed (during acceleration or deceleration), and there are intervals where the current remains constant to maintain that speed.

Due to actuator saturation, a reference peak exceeding the maximum allowable current  $i_{a,\text{max}}$  is not tracked by the controller, correctly applying the anti-windup principles.

We also note that during the start-up phase, armature current reaches a high value, but this is sustainable for our electrical machine since it persists for only a short duration, and is therefore permissible within our control scheme.

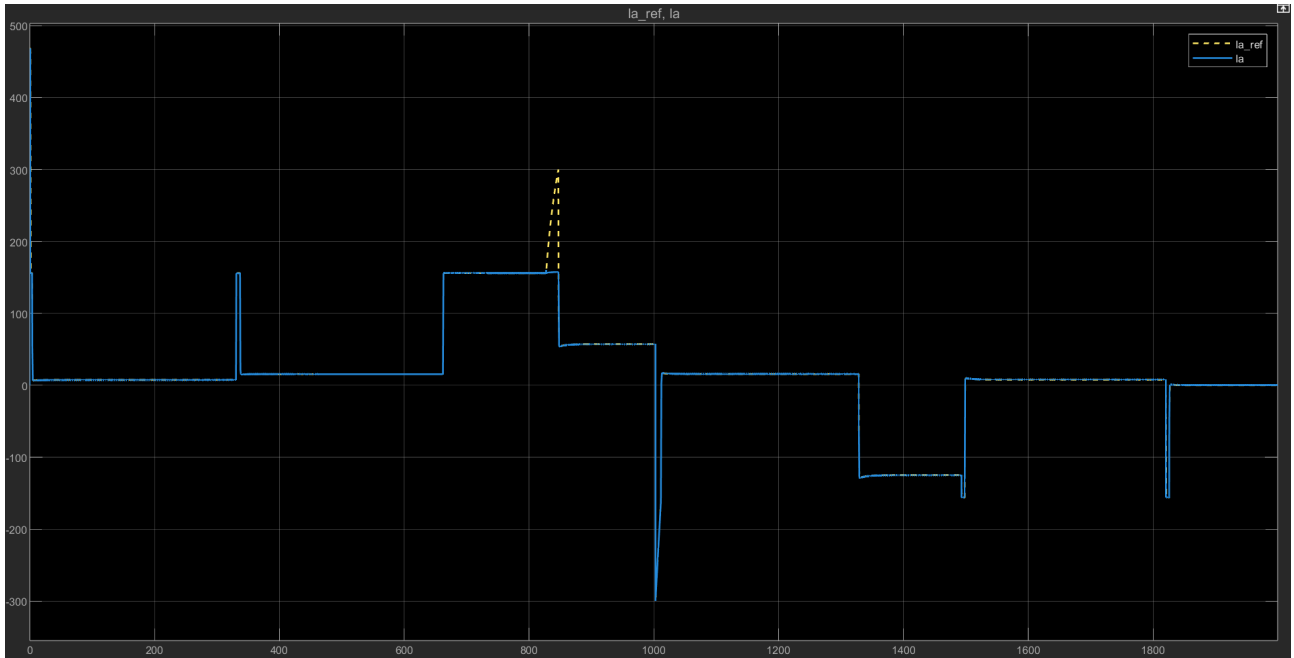


Figure 38: Desired armature current profile to follow (dashed yellow line) vs. measured armature current profile (blue line)

### 5.3. Excitation Current Control

According to the operating regions of the DC machine, the excitation current is maintained constant along the track, except when the tram enters its "*Field-Weakening Region*", where  $i_e$  (and thus  $V_e$ ) is reduced.

We also observe two small “inverse” peaks along the route, which are justified by the fact that the tram exceeded the base speed  $\Omega_b$  for a very brief interval.

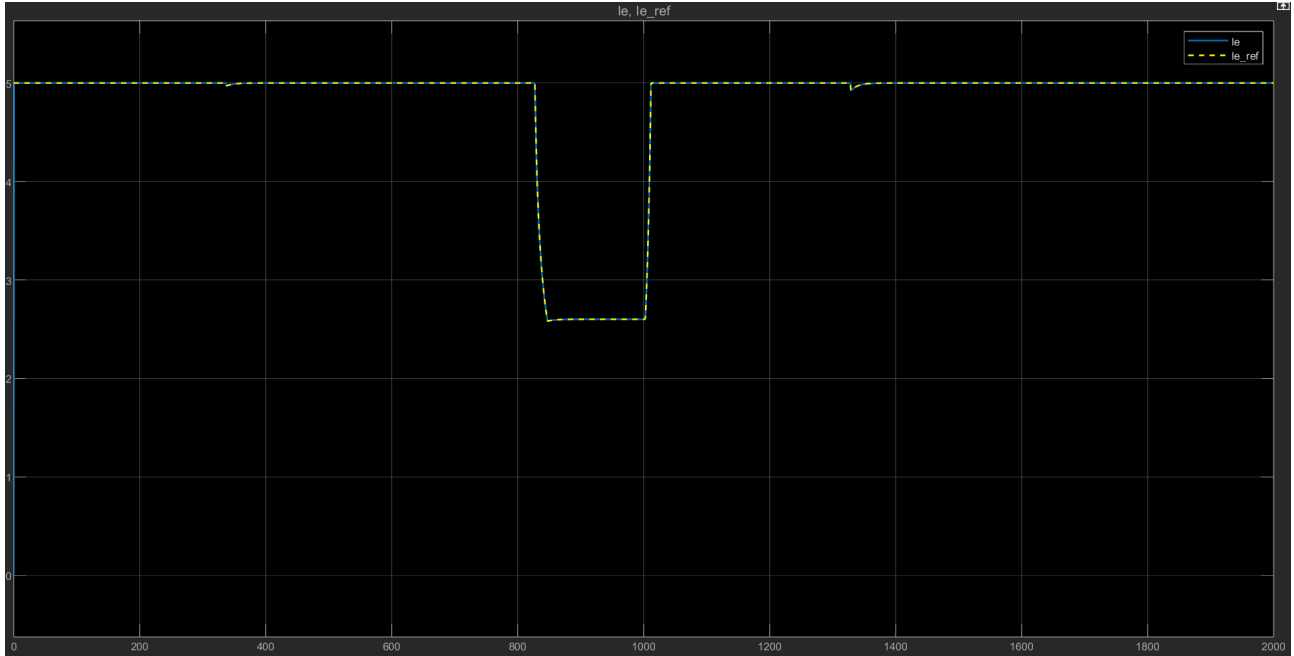


Figure 39: Desired excitation current profile to follow (dashed yellow line) vs. measured excitation current profile (blue line)

## 6. Matlab code

Below, we present the MATLAB code used to compute the missing parameters and tune the PI controller.

```

1 %excitation circuit parameters
2
3 Ve_r=60; %excitation rated voltage
4 Ie_r=5; %excitation rated current
5 Re=12; %excitation resistance
6 tau_e=0.1; %excitation time constant [s]
7 Le=tau_e*Re;
8
9
10 %other parameters
11
12 mt=15000; %mass of the vehicle at no load [Kg]
13 m_max=mt+130*80; %mass of the vehicle+added passengers at maximum loading capacity
14
15
16 ia_r=156; %overall rated current [A]
17 Pr_tot=21000*4; %total rated power for the equivalent DC motor [W]
18 Va_r=600; %line voltage=rated armature voltage (upper limit in the saturation block)
19
20 d= 680e-3; %diameter of the wheel [m]
21 rho=13/74; %gearbox ratio (motor-to-wheels)
22
23 v_max=42; %maximum speed of the vehicle [km/h]
24 omega_max=(v_max/3.6)*2/(d*rho); %maximum "structural" mechanical limit [rad/s]
25 omega_b=970*(2*pi/60); %[rad/s] rated angular speed of the motor (the base
   speed)-->at this speed we are applying the rated armature voltage
26 v_r=omega_b*rho*(d/2)*3.6; %rated linear speed
27
28
29 %machine parameters (ARMATURE PART)
30
31 Ra = 0.39;
32 tau_a = 10e-3; %time constant of the electrical part [s]
33 La = tau_a*Ra;
34 J = m_max*((rho^2*d^2)/4); %equivalent inertia seen by the motor, calculated in the
   WORST CASE SCENARIO (full loading capacity)
35 B = 0.81; %"beta"-->friction coefficient
36 Ks = 1.06; %called "Kt" in the dataset-->under some assumption the torque is
   considered equal to the back emf constant
37 Tn= Pr_tot/omega_b;
38 E_n=Ks*Ie_r*omega_b;
39
40 %% definition of the system TF
41
42 s = tf('s');
43
44 Gi = 1/(Ra+La*s); %electrical part
45 GO = 1/(B+J*s); %mechanical part
46
47 Ge = 1/(Re+Le*s); %excitation part
48
49
50 %imposition of the critical pulsations
51
52 wc_a=500;
53 wc_m=5;
54
55 wc_e=50;
56

```

```

57 %at the end the system must be stable, so we also request a high phase margin
      (>=80, avoiding oscillating dynamics)
58 phase_m_curr = 90;
59 phase_m_speed = 90;
60
61 phase_m_exc=90;
62
63
64 %% PID TUNER approach, to obtain the expression of the desired PI controller
      (imposing also the phase margin)
65 %re-writing the phase margin to insert it in the pidtune function
66 opt_curr = pidtuneOptions('PhaseMargin',phase_m_curr);
67 opt_speed = pidtuneOptions('PhaseMargin',phase_m_speed);
68
69 %CONTROLLER FOR EXCITATION PART (like the one of the electrical part, using Le and
      Re)
70 opt_exc_curr = pidtuneOptions('PhaseMargin',phase_m_exc);
71
72
73 [Ccurr, info_curr] = pidtune(Gi,'pi',wc_a,opt_curr); %we request a goal dynamic of
      wc_a and a phase margin opt_curr
74 [Cspeed, info_speed] = pidtune(G0,'pi',wc_m,opt_speed);
75
76 [Cexc_curr, info_exc_curr] = pidtune(Ge,'pi',wc_e,opt_exc_curr);
77
78 %we build up the obtained controllers
79 R_curr = Ccurr.Kp+Ccurr.Ki/s;
80 R_speed = Cspeed.Kp+Cspeed.Ki/s;
81
82 R_exc_curr = Cexc_curr.Kp+Cexc_curr.Ki/s;
83
84 %open loop TF
85
86 L_curr = R_curr*Gi;
87 L_speed = R_speed*G0;
88
89 L_exc_curr = R_exc_curr*Ge;
90
91 %closed loop TF (built in an independent way)
92
93 F_curr = feedback(L_curr,1);
94 F_speed = feedback(L_speed,1);
95
96 F_exc_curr = feedback(L_exc_curr,1);
97
98 %NESTING the speed controller and the speed TF around the closed loop TF of the
      current
99 %-->this is due to the COMPENSATION OF THE EMF ("E_est"), which generate an
      equivalent decoupled scheme
100 F_comp = feedback(R_speed*F_curr*G0,1);

```